# Impurity Ferromagnetism of Pd-Fe and Pd-Co Alloys: Ab Initio vs. Experiment [†]

**Alexandra Korableva [1], Irina Piyanzina [1,2,\*], Amir Gumarov [1,2], Igor Yanilkin [1,2] and Rustam Khaibullin [2]**

[1] Institute of Physics, Kazan Federal University, 420008 Kazan, Russia; alkorablewa@yandex.ru (A.K.); amir@gumarov.ru (A.G.); yanilkin-igor@yandex.ru (I.Y.)

[2] Zavoisky Physical-Technical Institute, FRC Kazan Scientific Center of RAS, 420029 Kazan, Russia; rikkfti@mail.ru

[\*] Correspondence: i.piyanzina@gmail.com

[†] Presented at the 3rd International Online-Conference on Nanomaterials, 25 April–10 May 2022. Available online: https://iocn2022.sciforum.net/.

**Abstract:** We have performed full-stack research of $Pd_{1-x}Fe_x$ and $Pd_{1-x}Co_x$ ($x = 0.01$–$0.1$) alloys. At the first stage, the occurrence of impurity ferromagnetism in considered alloys was studied employing the Density Functional Theory (DFT). At the second stage, magnetic impurities of Fe and Co atoms were implanted into epitaxial Pd thin films to verify DFT results. Magnetic properties of implanted Pd films were investigated by Vibrating Sample Magnetometer (VSM) in the temperature range from 5 K to 300 K. It has been established that VSM results are in a good agreement with ab initio calculations.

## 1. Introduction

The impurity ferromagnetism of strongly paramagnetic palladium aroused great interest among theoreticians and experimentalist back in the last century due to the fact that the effective magnetic moment per one magnetic impurity, for example, iron, turned out to be anomalously large, up to 12 Bohr magnetons [1–3]. To date, the revival of interest in Pd-Fe alloys was caused mainly by their potential use as a weak ferromagnet in superconducting magnetic random-access memory (MRAM) based on Josephson junctions [4–7]. Despite the long history of studies of such structures, the region of low impurity concentrations has not yet been sufficiently studied. Thus, recently, new features of the phase diagram of a palladium-iron alloy were discovered experimentally in the low concentration region, ≤10 at. %, in particular, it was demonstrated that ion implantation of iron into epitaxial palladium films can lead to the formation of a multiphase magnetic system [8–10]. Pd-Fe alloys synthesized by ion implantation with an average iron content in the range of 2–8 at. % are metastable with respect to ferromagnetism and formed phases. As a result of thermal annealing of the samples under high vacuum conditions, an increase in the magnetization of the films and an increase in the Curie temperature were observed, as well as the formation of additional stable phases. In addition, some discrepancies were found with older works from this area [11].

Theoretical calculations could help correlate recent results with older work and shed light on the mechanisms of magnetization formation in palladium-iron alloys. This project is based on fundamental studies of the structural and magnetic properties of $Pd_xA_{1-x}$ alloys ($x \leq 10$ at. %, A = Fe and Co) using computer simulation within the framework of the density functional theory (DFT). Theoretical investigation has been performed in a close

collaboration with an experimental group dealing with the growth and analysis of thin films. In the present paper DFT results will be presented along with Vibrating Sample Magnetometer (VSM) measurements for both Pd-Fe and Pd-Co alloys with an impurity content of up to 10 at. %.

## 2. Materials and Methods

### 2.1. DFT Calculation Details

In the present paper ab initio investigations were based on the DFT [12,13] within the VASP code [14–16] as a part of the MedeA® software of Materials Design [17]. Exchange and correlation effects were accounted for by the generalized gradient approximation (GGA) as parameterized by Perdew, Burke, and Ernzerhof (PBE) [18]. The Kohn–Sham equations were solved using the plane–wave basis set (PAW) [19]. The cut-off energy was chosen to be equal to 400 eV. The force tolerance was 0.5 eV/nm and the energy tolerance for the self-consistency loop was $10^{-5}$ eV. The Brillouin zones were sampled using Monkhorst–Pack grids [20], including $3 \times 3 \times 3$ k-points. We performed spin-polarized calculations in all cases, initializing Fe and Co atoms to have 3.63 and 1.5 $\mu_B$, respectively, and Pd atoms to be in the paramagnetic state (0 $\mu_B$). The structures are described as consisting of a filled FCC host matrix formed by Pd atoms, with Fe and Co ions substituting octahedrally coordinated sites only (as shown in Figure 1). For the $3 \times 3 \times 3$-unit cell parameter a = 11.8 Å.
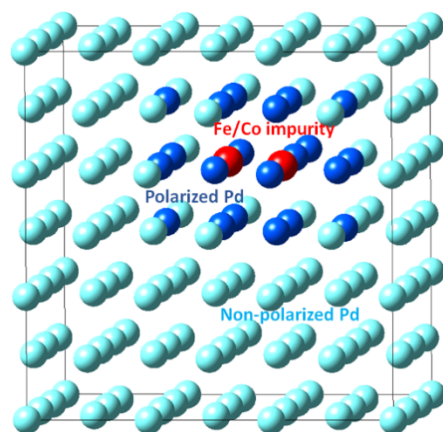


**Figure 1.** Supercell of Pd matrix used in our calculations with denoted polarized Pd atoms around the Fe or Co solute ions after the optimization procedure. Red sphere of atom corresponds to Fe/Co, light blue to Pd, and blue to predominantly polarized Pd atoms.

### 2.2. The Experiment Description

The epitaxial Pd films were produced by molecular-beam epitaxy (MBE) in ultrahigh vacuum conditions of $5 \times 10^{-10}$ mbar on epi-ready ($R_a < 0.5$ nm) (100)-MgO single-crystal with dimensions of $5 \times 10 \times 0.5$ mm³ provided by Crystal GmbH, Berlin Germany. Pd were evaporated from Createc Fischer effusion cell with precise temperature control of ±0.1 °C. During the deposition process, the temperature of the Pd was constant (1305 °C) and the growth rate was 11.4 nm/hour. Film growth was carried out in three stages (by analogy with the work in Ref. [8]). At the first stage, the substrate temperature was 400 °C and the first layer of 10 nm thick was deposited. At the second stage, the substrate temperature was 150 °C and final layer of 30 nm thick was deposited. Finally, the film was annealed in vacuum at a temperature of 600 °C for 20 min. The structural perfection of the film was monitored in situ at each stage by low-energy electron diffraction and ex situ by X-ray diffraction. A series of 40 nm epitaxial Pd films were grown under the same conditions. Then samples were taken out of the vacuum for further ion implantation procedure. 40 keV Fe⁺ (or Co⁺) ions were implanted with different doses (determines the impurity

content) into fresh-grown epitaxial Pd films. Thus, two series of samples were synthesized, which differed from each other in the implanted type of chemical impurity (see Table 1). Synthesized by ion implantation Pd-Fe and Pd-Co alloy films were additionally annealed in ultrahigh vacuum ($9 \times 10^{-9}$ mbar) at a temperature of 600 °C for 2 h. Such annealing was carried out to make the samples stable and get rid of radiation defects. After annealing all samples were cut into several parts using a diamond saw with a non-magnetic base, and one piece of each sample were measured by VSM in the temperature range from 5 K to 300 K.

**Table 1.** Experimental samples synthesized by implantation of $Fe^+$ (or $Co^+$) ions into epitaxial Pd films.

| Sample | Implanted Ion | Implantation Energy (keV) | Dose ($\times 10^{16}$ ions/cm$^2$) |
|---|---|---|---|
| FePd-1 | | | 0.5 |
| FePd-2 | Fe | 40 | 1.0 |
| FePd-3 | | | 3.0 |
| CoPd-1 | | | 0.5 |
| CoPd-2 | Co | 40 | 1.0 |
| CoPd-3 | | | 3.0 |

## 3. Results

### 3.1. DFT Calculations

Fe impurity in the Pd matrix has been investigated in our previous research [21]. Here we focus on the comparison with Co impurity. The calculated total magnetization per impurity is shown in Figure 2 versus impurity content. At low impurity concentration ($x$ = 0.01 to $x$ = 0.03 for Fe and to $x$ = 0.02 for Co) we got a negligible cell magnetization. At such low concentrations Co and Fe are non-magnetic. The average magnetization of impurities versus impurity content is shown in Figure 3. As was discussed in our previous research [21] the low-concentration regions behavior, in particular zero magnetic moments, is in consistence with theory of impurity ferromagnetism [22]. However, as was shown previously for Fe impurity, there is a discrepancy in the low-concentration region between ab initio and experiments (Figure 2a in Ref. [21]). That might be since the calculations were performed assuming 0 K, and we obtained Fe and Co solute atoms after optimization as being non-magnetic at low impurity concentrations, whereas experimental measurements were carried out at final temperatures.
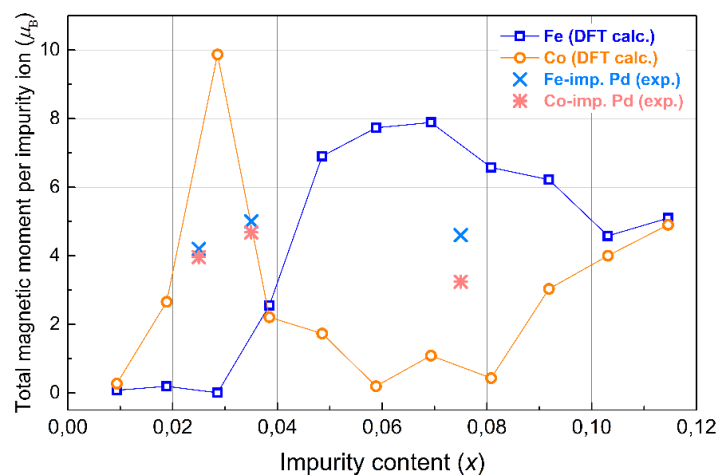


**Figure 2.** Total magnetization of $Pd_{1-x}Fe_x$ and $Pd_{1-x}Co_x$ ($x$ = 0.01–0.1) systems calculated per impurity atom versus impurity content in the 3 × 3 × 3 Pd supercell.
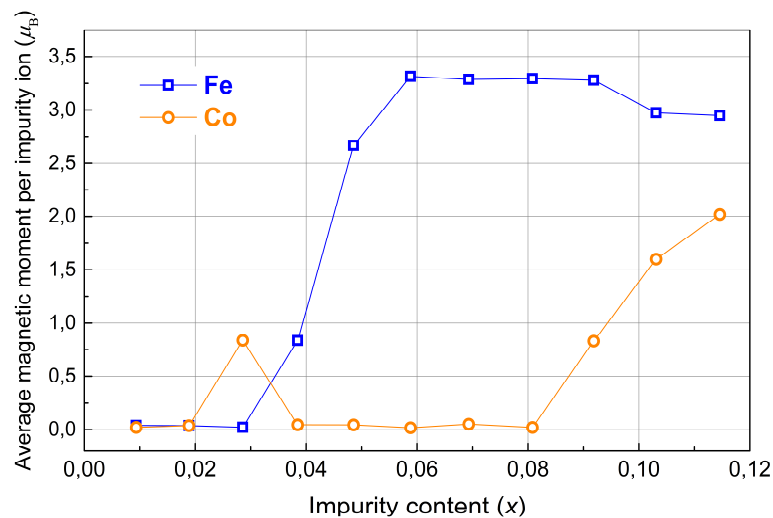
**Figure 3.** Calculated average magnetization of Fe and Co in Pd$_{1–x}$Fe$_x$ and Pd$_{1–x}$Co$_x$ ($x$ = 0.01–0.1) systems versus impurity content in the 3 × 3 × 3 Pd supercell.

At the concentrations above $x$ = 0.03 for Fe and $x$ = 0.02 for Co total magnetization along with impurity magnetic moments and maximal Pd magnetic moments (as shown in Figure 4) increase reaching the maximum of total magnetization per impurity being equal to ~8 $\mu_B$ for Fe and ~10 $\mu_B$ for Co. The calculated averaged magnetization of impurities for Fe reaches a plateau with a constant value of ~3.25 $\mu_B$ (Figure 3) which is lower than the theoretical maximum, but it is higher than the value of 2.8 $\mu_B$ obtained in [1] and close to the value of 3.5 $\mu_B$ obtained by Neutron diffraction experiments [23,24]. For Co it was obtained that maximum of total magnetization is higher than for Fe (Figure 2). That value agrees well with saturation moment published in Table 2.1 of Ref. [2] above 0.07 at. %. However, in according with mentioned data, magnetization value stays constant up to 0.5 at. %, whereas ab initio calculations show rapid decline of the curve (Figure 2). After the peak point the Fe-curve decreases very slow in agreement with experiments and theoretical predictions [21]. In contrast after the concentration of $x$ = 0.09 the Co-curve goes up again. In the further calculations the concentrations above $x$ = 0.11 will be checked along with the low-concentration region to ensure such a non-expected behavior. On the other hand, at higher concentrations both Fe and Co curves are getting closer (Figures 2–4), what might be the reassurance of correct results.

### 3.2. Magnetostatic Measurements

The static magnetic properties of the Fe- and Co-implanted Pd films were measured utilizing the vibrating sample magnetometry (VSM) in the temperature range of 5–300 K with the magnetic field applied either in-plane or out-of-plane of the films. To determine the $M_s$ of the Pd-Fe and Pd-Co alloy films, the net diamagnetic contribution of the MgO substrate was subtracted from the raw VSM data. Then, the saturation magnetic moment $M_s$ was recalculated to the number of Bohr magnetons ($\mu_B$) per implanted Fe$^+$ or Co$^+$ ion. As expected, the magnitude of the $M_s$ and the Curie temperature will increase with an increase in the implantation dose (impurity concentration). Note, that the average impurity concentration in implanted samples was taken from experimental distribution profiles obtained by X-ray phoroelectron spectroscopy in combination with sequential Ar-ion etching of the sample surface (profiles are not presented here) and for the doses of 0.5, 1.0, and $3.0 \times 10^{16}$ ions/cm$^2$ were corresponded to $x$ = 0.025, $x$ = 0.035, and $x$ = 0.075, respectively. Figure 5 shows magnetic hysteresis loops for the FePd-3 and CoPd-3 samples. It is clearly seen that the magnetic hysteresis loops recorded for Pd films implanted with Fe$^+$ or Co$^+$ ions differ significantly in the magnitude of the $M_s$, magnetic anisotropy and coercive field ($H_c$). A significant difference is observed in the magnitude of the $H_c$ for Co-implanted Pd

film (CoPd-3), this value is ~1300 Oe, while for the FePd-3 this value is just ~9 Oe (Figure 5). Such a difference in the magnitude of the $H_c$ is associated with a fundamental difference in the magnetocrystalline anisotropy of iron and cobalt impurities. Moreover, the $H_c$ of Co-implanted Pd films significantly depends on the implantation dose (Co concentration), in particular, for CoPd-2 it is ~700 Oe and for CoPd-1 it is ~250 Oe.
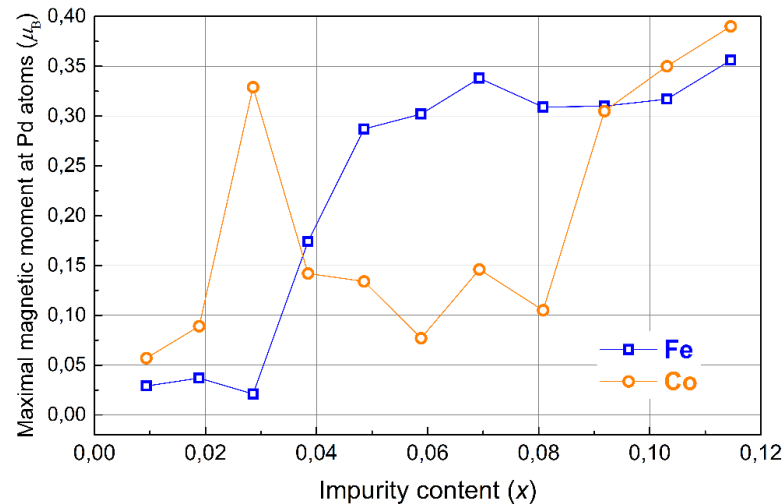


**Figure 4.** Maximal calculated magnetic moment at Pd atom in $Pd_{1-x}Fe_x$ and $Pd_{1-x}Co_x$ ($x$ = 0.01–0.1) systems versus impurity content in the 3 × 3 × 3 Pd supercell.
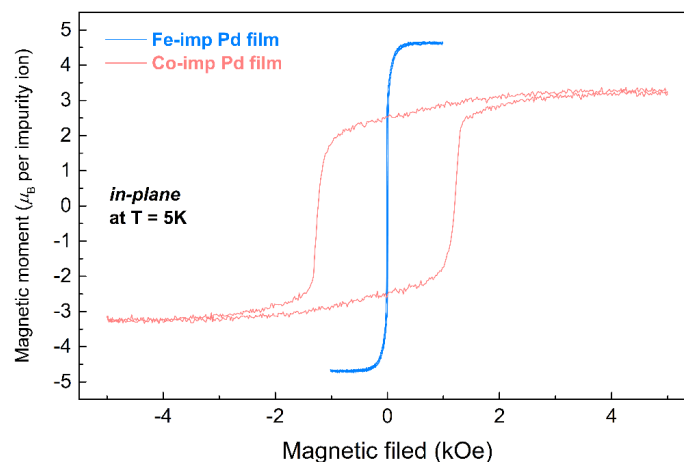


**Figure 5.** Magnetic hysteresis loops for 40 nm epitaxial Pd film implanted by Fe+ ions (blue curve) or Co+ ions (red curve) with the dose of $3.0 \times 10^{16}$ ions/cm2.

## 4. Discussion and Conclusions

Comparison of experimental data and theoretical calculation of the concentration dependences of the magnetization of Pd-Fe and Pd-Co alloys with an impurity content of up to 10 at. % showed their qualitative agreement with each other. At similar concentrations of magnetic impurity in the palladium matrix, in the experiment and in the calculation, a maximum of the magnetic moment per impurity was observed. In this case, the observed differences between the calculated and experimental data may be due to the fact that the magnetic impurity is distributed inhomogeneously in the implanted palladium matrix [11]. The cumulative analysis of the obtained data suggests that DFT method can be used to study Pd-Fe and Pd-Co alloys.

## References

1. Crangle, J. Ferromagnetism in Pd-rich palladium-iron alloys. *Philos. Mag.* **1960**, *5*, 335–342.
2. Nieuwenhuys, G.J. Magnetic behaviour of cobalt, iron and manganese dissolved in palladium. *Adv. Phys.* **1975**, *24*, 515–591.
3. Wohlfarth, E.P. *Handbook of Magnetic Materials*; North-Holland Publishing Company: London, UK, 1980; Volume 1, p. 75.
4. Ryazanov, V.V. Josephson superconductor—ferromagnet—superconductor $\pi$-contact as an element of a quantum bit (experiment). *Uspekhi Fiz. Nauk* **1999**, *42*, 825–827.
5. Larkin, T.I.; Bol'ginov, V.V.; Stolyarov, V.S.; Ryazanov, V.V.; Vernik, I.V.; Tolpygo, S.K.; Mukhanov, O.A. Ferromagnetic Josephson switching device with high characteristic voltage. *Appl. Phys. Lett.* **2012**, *100*, 222601.
6. Ryazanov, V.V.; Bol'ginov, V.V.; Sobanin, D.S.; Vernik, I.V.; Tolpygo, S.K.; Kadin, A.M.; Mukhanov, O.A. Magnetic Josephson junction technology for digital and memory applications. *Phys. Procedia* **2012**, *36*, 35–41.
7. Vernik. I. V.; Bol'ginov, V.V.; Bakurskiy, S.V.; Golubov, A.A.; Kupriyanov, M.Y.; Ryazanov, V.V.; Mukhanov, O.A. Magnetic Josephson junctions with superconducting interlayer for cryogenic memory. *IEEE Trans. Appl. Supercond.* **2013**, *23*, 1701208.
8. Esmaeili, A.; Yanilkin, I.V.; Gumarov, A.I.; Vakhitov, I.R.; Yusupov, R.V.; Tatarsky, D.A.; Tagirov, L.R. Epitaxial thin-film $Pd_{1-x}Fe_x$ alloy—A tunable ferromagnet for superconducting spintronics. *Sci. China Mater.* **2021**, *64*, 1246–1255.
9. Mohammed, W.M.; Yanilkin, I.V.; Gumarov, A.I.; Kiiamov, A.G.; Yusupov, R.V.; Tagirov, L.R. Epitaxial growth and superconducting properties of thin-film PdFe/VN and VN/PdFe bilayers on MgO(001) substrates. *Beilstein J. Nanotechnol.* **2020**, *11*, 807–813.
10. Yanilkin, I.V.; Mohammed, W.M.; Gumarov, A.I.; Kiiamov, A.G.; Yusupov, R.V.; Tagirov, L.R. Synthesis, characterization, and magnetoresistive properties of the epitaxial $Pd_{0.96}Fe_{0.04}/VN/Pd_{0.92}Fe_{0.08}$ superconducting spin-valve heterostructure. *Nanomaterials* **2021**, *11*, 64.
11. Gumarov, A.I.; Yanilkin, I.V.; Yusupov, R.V.; Kiiamov, A.G.; Tagirov, L.R.; Khaibullin, R.I. Iron-implanted epitaxial palladium thin films: Structure, ferromagnetism and signatures of spinodal decomposition. *Mater. Lett.* **2021**, *305*, 130783.
12. Hohenberg, P.; Kohn, W. Inhomogeneous Electron Gas. *Phys. Rev.* **1964**, *136*, B864–B871.
13. Kohn, W.; Sham, L.J. Self-Consistent Equations Including Exchange and Correlation Effects. *Phys. Rev.* **1965**, *140*, A1133–A1138.
14. Kresse, G.; Furthmüller, J. Efficiency of ab-initio total energy calculations for metals and semiconductors using a plane-wave basis set. *Comp. Mat. Sci.* **1996**, *6*, 15–50.
15. Kresse, G.; Furthmüller, J. Efficient iterative schemes for ab initio total-energy calculations using a plane-wave basis set. *Phys. Rev. B* **1996**, *54*, 11169–11186.
16. Kresse, G.; Joubert, D. From ultrasoft pseudopotentials to the projector augmented-wave method. *Phys. Rev. B* **1999**, *59*, 1758–1775.
17. *MedeA*, version 3.4; MedeA is a Registered Trademark of Materials Design, Inc.: San Diego, CA, USA, 2021.
18. Perdew, J.P.; Burke K.; Ernzerhof, M. Generalized Gradient Approximation Made Simple. *Phys. Rev. Lett.* **1996**, *77*, 3865–3868.
19. Blöchl, P.E. Projector augmented-wave method. *Phys. Rev. B* **1994**, *50*, 17953–17979.
20. Monkhorst, H.J.; Pack, J.D. Special points for Brillouin-zone integrations. *Phys. Rev. B* **1976**, *13*, 5188–5192.
21. Piyanzina, I.; Gumarov, A.; Khaibullin, R.; Tagirov, L. Ab initio Investigation of Impurity Ferromagnetism in the $Pd_{1-x}Fe_x$ Alloys: Concentration and Position Dependences. *Crystals* **2021**, *11*, 1257.
22. Korenblit, I.Y.; Shender, E.F. Ferromagnetism of disordered systems. *Sov. Phys. Uspekhi* **1978**, *21*, 832–851.
23. Low, G.G. The electronic structure of some transition metal alloys. *Adv. Phys.* **1969**, *18*, 371–400.
24. Aldred, A.T.; Rainford, B.D.; Stringfellow, M.W. Magnetic Moment Distribution in Dilute Alloys of Nickel in Palladium. *Phys. Rev. Lett.* **1970**, *24*, 897–900.